Hindawi
Journal of Food Quality
Volume 2018, Article ID 1809297, 10 pages
https://doi.org/10.1155/2018/1809297

Research Article

Nondestructive Identification of Salmon Adulteration with Water Based on Hyperspectral Data

Tao Zhang,[1,2] Biyao Wang,[1,2] Pengtao Yan,[1,2] Kunlun Wang,[1,2] Xu Zhang,[1,2] Huihui Wang,[1,2] and Yan Lv[1,2]

[1]*Engineering Research Center of Seafood, Dalian 116034, Liaoning, China*
[2]*School of Mechanical Engineering and Automation, Dalian Polytechnic University, Qinggongyuan1, Ganjingzi District, Dalian 116034, Liaoning, China*

Correspondence should be addressed to Xu Zhang; 11587669@qq.com and Huihui Wang; 1009960774@qq.com

Received 11 September 2018; Revised 24 November 2018; Accepted 10 December 2018; Published 26 December 2018

Academic Editor: Daniel Cozzolino

Copyright © 2018 Tao Zhang et al. This is an open access article distributed under the Creative Commons Attribution License, which permits unrestricted use, distribution, and reproduction in any medium, provided the original work is properly cited.

For the identification of salmon adulteration with water injection, a nondestructive identification method based on hyperspectral images was proposed. The hyperspectral images of salmon fillets in visible and near-infrared ranges (390–1050 nm) were obtained with a system. The original hyperspectral data were processed through the principal-component analysis (PCA). According to the image quality and PCA parameters, a second principal-component (PC2) image was selected as the feature image, and the wavelengths corresponding to the local extremum values of feature image weighting coefficients were extracted as feature wavelengths, which were 454.9, 512.3, and 569.1 nm. On this basis, the color combined with spectra at feature wavelengths, texture combined with spectra at feature wavelengths, and color-texture combined with spectra at feature wavelengths were independently set as the input, for the modeling of salmon adulteration identification based on the self-organizing feature map (SOM) network. The distances between neighboring neurons and feature weights of the models were analyzed to realize the visualization of identification results. The results showed that the SOM-based model, with texture-color combined with fusion features of spectra at feature wavelengths as the input, was evaluated to possess the best performance and identification accuracy is as high as 96.7%.

1. Introduction

Salmon is rich in nutrition, especially unsaturated fatty acids, which can eliminate the cholesterol and lipids in human blood, lowering the incidence of cardiovascular disease [1]. With the rapid development of the salmon industry, the adulteration of salmon has become a serious concern in China. Some merchants profit by injecting water into salmon to increase the weight. Because of the injection, the taste of salmon gets worse and the microbial content in salmon exceeds the limit of the standards, resulting in the harm to human health [2]. For the detection of salmon quality, artificial evaluation and physiochemical detection have been applied. The former is not objective, not quantitative, and not safe enough, restricting the automation and intelligence in the food processing industry. Some traditional physical and chemical detection methods have the advantages of simplicity and low cost, but most of these methods are destructive, time-consuming, and highly professional [3, 4]. For the detection of water, nuclear magnetic resonance can obtain direct information about interactions between hydrogen protons and exchangeable protons in proteins and hence the chemical and physical state of water, especially in muscle and meat [5]. However, the testing instrument is expensive and mainly used at the laboratory testing level in food detection. Therefore, it is necessary to explore a fast, nondestructive, and convenient detection technique for the identification of adulterated salmon and other foods [6].

In recent years, spectrum-based nondestructive detection technologies have been developed [7], as more effective alternatives to traditional detection methods. Based on the acquisition and analysis of spectral information, the apparent quality and composition of samples can be better

learned. Among these spectral technologies, hyperspectral imaging technology can derive a large amount of imaging information at continuous spectral wavelengths and at varied spatial dimensions. Namely, the spectral data contain three-dimensional information, which are spectrum and image dimensional. The extraction and analysis of these spectral data at feature wavelengths have shown great advantages in the detection of food quality [8, 9]. For the samples with different chemical compositions and structures, the absorbance, reflectivity, and dispersion corresponding to the feature wavelengths are different. Especially, the samples with different chemical compositions show unique absorbance results at feature wavelengths due to their functional groups [10]. Accordingly, the quantitative studies on the chemical compositions of samples, identification and detection of food quality, and visualization expression of detection information can be realized through the analysis of the images and spectral data acquired [11]. The hyperspectral images contain abundant data information. Each pixel in a two-dimensional image contains spectral information at thousands of wavelengths. The hyperspectral technology can achieve both collinearity elimination and full information acquisition simultaneously, which is impossible in traditional spectral methods [12]. Combining chemometrics, intelligent algorithms, and so forth, the hyperspectral technology can visualize the inner and outer information of the samples [13] and can nondestructively and accurately determine the component, content, state, and spatial distribution of the samples [14]. In view of these merits, this technology has been widely applied in the field of nondestructive quality detection of food such as vegetables [15], fruits [16], seafood [17], milk [18], honey [19], etc., [20]. In particular, the technique has received a considerable attention in meat quality, safety, and authenticity. Their applications include quantifying the adulteration level of minced lamb meat with pork [21], detecting horsemeat adulteration in minced beef [22], examining gelatin adulteration in shrimp and crab adulteration with the imitation crab meat mainly based on surimi [23, 24]. Because of the huge amount of information in hyperspectral data, currently, this detection technology usually combines with statistical algorithms [25], on the basis of effective data dimensionality reduction processing [26], to realize the high-efficiency quantitative analysis and identification of products' quality [27, 28].

In this study, the hyperspectral images and spectral information of water-adulterated salmon were acquired. Then, the data dimensionality reduction was realized with the principal-component analysis (PCA). The texture information, color information, and feature-wavelength spectral data of principal-component images were extracted, for the establishment of an SOM-based water-adulterated salmon quality identification model.

2. Materials and Methods

2.1. Materials. Salmon samples, 2 cm × 1 cm × 1 cm, were purchased from a WAL-MART supermarket in Dalian, China. The samples are fresh meat without skin and bones. Sixty samples from different salmon parts (belly and back) were dried at 105°C to a constant weight in an oven for water content determination. The water content of salmon samples ranges from 64 to 73% approximately, and the standard deviation was 0.048. Then, the salmon, stored in a refrigerator at 4°C, was transported to our laboratory. Before the test, the salmon was injected with a certain amount of water. It was found that the upper injection limit was 0.6 mL if water seepage, color change, and texture change of the sample could not be observed by naked eyes. Therefore, according to the injection amount, the salmon samples were divided into four groups: the first was salmon without water injection; the second was salmon with 0–0.2 mL (small amount) of water injected; the third was salmon with 0.2–0.4 mL (moderate amount) of water injected; and the fourth was salmon with 0.4–0.6 mL (large amount) of water injected. One-hundred samples were used for the model building, of which 60 samples were used as the modeling set and 40 samples were used as the prediction set. Each group of the modeling set included 15 samples, and these were numbered to be 1–15, 16–30, 31–45, and 46–60, respectively. Each group of the prediction set included 10 samples, and these were numbered to be P1–P10, P11–P20, P21–P30, and P31–P40, respectively.

2.2. Hyperspectral Data Acquisition. The hyperspectral data were acquired with a hyperspectral imaging system (Sichuan Dualix Spectral Image Technology Co. Ltd.). The system was mainly composed of an Image-λ-V10E-LU-enhanced vis-near-infrared hyperspectral camera, spectrometer, halogen light source, and electronically controlled mobile platform. The available spectral range was 379–1038 nm. For the acquirement of undistorted, real, and clear hyperspectral imaging data, the experimental parameters were set as follows: the spectral resolution was 2.8 nm, exposure time was 10 ms, object distance was 50 cm, moving speed of the platform was 5 mm/s, spectral sampling points were 0.65 nm in diameter, and wavelength was in the range of 379–1038 nm.

2.3. Hyperspectral Image Correction. To reduce the difference between the illumination and camera dark current in different samples, we conducted the black and white board correction before the acquisition of all spectral images [29]. In detail, a white calibration image W (reflectivity approaching 100%) was first obtained by scanning a standard white calibration board. Then, all light sources and camera lens were closed to collect a black calibration image D (reflectivity approaching 0%). The original hyperspectral image could be corrected as follows [30]:

$$R = \frac{R_0 - D}{W - D} \times 100\%, \quad (1)$$

where R represents the corrected hyperspectral image; R_0 stands for the original hyperspectral image; W represents the white calibration image; and D represents the black calibration image.

2.4. Extraction of Spectral Data and Data Dimensionality Reduction. A region with the size of 50 × 50 pixels^2 in the middle of a salmon image was selected as the region of interest (ROI) for the extraction and analysis of spectral, texture, and color features of this image. On this basis, the prediction model for salmon quality detection was established. A 3 × 3 pixels^2 smoothing window was selected to smooth the average spectral profiles with the Savitzky–Golay (SG) method to remove high-frequency noises and to improve the signal-to-noise ratio [31]. Because the amount of data acquired by hyperspectra was large, we applied the PCA method to reduce the dimensionality of the hyperspectral data [32]. The eigenvalues and cumulative contribution rates of the first six principal-component images were calculated. According to the imaging quality of these six principal-component images, one of the images was screened for further analysis [33].

The principal-component image is the linear combination of the original images at different wavelengths. The coefficient of an image at a specific wavelength is the so-called weighting coefficient. A local extremum of the weighting coefficients indicates that the hyperspectral image at this wavelength has a large contribution rate to the principal-component image [34, 35], and the corresponding wavelength will be chosen as a feature wavelength for subsequent research.

An ENVI v4.7 system (Research System, Inc., Boulder, CO, USA) was employed to extract the ROI and corresponding average spectral profile and to analyze the principal component of the image. MATLAB 2012a (the MathWorks Inc., Natick, MA, USA) software was used for the SG smoothing.

2.5. Texture Feature. Gray-level cooccurrence matrix is a matrix function of pixel distance and angle. Through the calculation of the correlation between the gray levels of two pixels in a certain distance and direction in an image, one can obtain the comprehensive texture information of a hyperspectral image from aspects of direction, interval, amplitude, and speed [36]. Suppose that $f(x, y)$ is a hyperspectral image of water-adulterated salmon, with the image size of $M \times N$ and gray level of Nr, a hyperspectral gray-level cooccurrence matrix in agreement with a certain spatial relationship can be established as follows [37, 38]:

$$P(m,n) = \rho\Big\{(x_1, y_1), (x_2, y_2)\varepsilon M \times N \big| f(x_1, y_1) = m, f(x_2, y_2) = n\Big\}, \tag{2}$$

where $\rho(x)$ represents the number of elements in the set x, P is an $M \times N$ matrix. Assuming that the distance between the two pixels in the salmon hyperspectral image is d and the difference between the angles between both pixels and the horizontal axis is θ, the gray-level cooccurrence matrix $P(m, n, d, \theta)$ with different distances and angles can be obtained [39]. In this paper, the cooccurrence matrices in four directions of 0°, 45°, 90°, and 135° were calculated with the centered pixel at the distance value of one. The contrast (CON), correlation (COR), entropy (ENT), energy (ENE), and angular second-order moment (ASM) of the ROI in these four directions were extracted, and the mean values were calculated as the texture features for the water-adulterated salmon identification model [40]. The calculation processes are presented as follows:

$$\begin{aligned}
\mathrm{CON} &= \sum_{i=0}^{M}\sum_{j=0}^{N}(i-j)^2 p(i,j),\\
\mathrm{CON} &= \sum_{i=0}^{M}\sum_{j=0}^{N}\frac{(i-\alpha)(j-\alpha)p(i,j)}{\beta^2},\\
\mathrm{ENT} &= -\sum_{i=0}^{M}\sum_{j=0}^{N}p(i,j)\lg p(i,j),\\
\mathrm{ENE} &= \sum_{i=0}^{M}\sum_{j=0}^{N}p(i,j),\\
\mathrm{ASM} &= \sum_{i=0}^{M}\sum_{j=0}^{N}p^2(i,j),\\
\alpha &= \sum_{i=0}^{M}\sum_{j=0}^{N}i\cdot p(i,j),\\
\beta^2 &= \sum_{i=0}^{M}\sum_{j=0}^{N}(i-\alpha)^2 p(i,j).
\end{aligned} \tag{3}$$

2.6. Color Moment Feature. Color moment is a method to measure the difference between images through color values. The image features based on color moment can well express the distribution of color values in images. A large number of statistical experiments have proven that the color distribution information of images can be well expressed via the corresponding low-order moments [41]. Therefore, the first- and second-order moments of the hyperspectral images of salmon were extracted and used as the color features for the water-adulterated salmon identification model:

$$\mu_i = \frac{1}{N}\sum_{i=1}^{N}P_i, \tag{4}$$

where μ is the first-order color moment of a hyperspectral image, representing the mean value of color; P_i represents the brightness value of a pixel i. N corresponds to the total number of pixels of the image:

$$\sigma_i = \left[\frac{1}{N}\sum_{j=1}^{N}\left(P_{ij} - \mu_i\right)^2\right]^{1/2}, \tag{5}$$

where σ_i represents the first-order color moment of a hyperspectral image, reflecting the standard deviation of the pixel values of the image.

2.7. Modeling for the Identification of Adulteration with Water. An identification model of salmon adulteration was established based on the self-organizing feature mapping (SOM). This model consisted of two layers of neurons: the upper layer was the output layer and the lower layer was the input layer. The input layer was actually a two-dimensional node matrix [42]. Each node represents a neuron [43]. The feature spectra (spectral values) with color moment features, texture features, and color moment and texture features were set as the input for modeling, respectively; each neuron in the input layer was connected with each other neurons in the output layer through the weight. Comparing with the different input model, forty salmon samples were used as a prediction set for the model which has the best performance in identification. On the other hand, the neurons in the output layer included four nodes, respectively, corresponding to the sample without water injected, with a small amount of water, with a moderate amount of water, and a large amount of water. The topological function of this model was the "hextop", the distance function was the "linkdist", and the number of iterations was set to be 1000 times.

3. Results and Discussion

3.1. Analysis of Hyperspectral Features for the Identification of Salmon Adulteration with Water. Figure 1(a) shows the averaged spectral profiles of salmon samples. These profiles of salmon with different water amounts injected exhibit similar shapes and trends. With the increasing of water amount injected, the spectral values at different wavelengths increased. Two obvious absorption bands at 400–600 nm were observed, probably due to the large G (green) and B (blue) values on the surfaces of the samples [44, 45]. Another absorption band was observed at 900–1000 nm. According to the literature, this band at 970 nm corresponds to the stretching vibration of O-H, which is related to the water in samples [46]. The original averaged spectral profiles contained many noises, which have a great negative impact on the spectral dimensionality reduction and features extraction accuracy [47]. Hence, SG smoothing was applied to remove noises, and the denoised profiles are shown in Figure 1(b). Most of the profiles were successfully smoothed, and the waveforms were not shifted or distorted. However, the part of noises in the ranges of 388–400 nm and 1000–1045 nm, caused by the low accuracy of the instrument, could not be eliminated. Therefore, the following studies only focused on the spectra and images in the range of 400–1000 nm.

3.2. Selection of Feature Images. After the analysis of spectral profiles, the images in the range of 400–1000 nm were treated with the PCA approach, and six principal components were derived as the output at each wavelength [48]. For instance, the principal-component feature values and contribution rates at feature wavelengths of the sample containing 0.3 mL of water are shown in Table 1. The eigenvalues PC1 and PC2 are greater than 1. The cumulative contribution rates of PC1 and PC2 are 85.2% and 96.0%, respectively. The cumulative contribution rate of the first two principal-component images surpassed 90%, indicating that these principal-component images could represent most of the information of the sample. Figure 2 shows the first six principal-component images of the sample. The first three principal-component images are clear, and the last three contain many noises, failing in the analysis and extraction of features. However, the brightness of the first principal-component image was too high to identify the water amount injected. The second principal-component image exhibited an obvious muscle texture, and the gray-level values of the injection region were higher than those of other regions. In conclusion, the image PC2 could be used for the analysis and extraction of image features. Figure 3 shows the second principal-component images of salmon samples with different water amounts injected. The gray-level values of the injection regions were largely decreased with the increase of water injection amount, showing that the response to water injection in the image PC2 was indicated by a lower pixel gray value. Thereby, the image color and texture of the injection regions changed with the different water amounts injected.

3.3. Selection of Feature Wavelengths. The weighting coefficients of the feature image (PC2) of salmon samples with 0, 0.2, 0.4, and 0.6 mL of water injected are illustrated in Figure 4. Local extremum values of weighting coefficients were observed at 454.9, 512.3, and 569.1 nm, indicating that these three wavelengths contributed more to the PC2 images and contained most of the feature information. Therefore, these three wavelengths were selected as the feature wavelengths for spectra extraction. The extracted spectra served as the input to establish the identification model of salmon adulteration.

3.4. Modeling for Identification of Water-Adulterated Salmon

3.4.1. Water-Adulterated Salmon Identification Model Based on the Color Moment Features and Feature Spectra. The features of the first- and second-order color moments and spectral values at feature wavelengths (454.9, 512.3, and 569.1 nm) of 60 salmon samples were extracted and normalized. The normalized data were used as the input for the SOM network [49] to establish an identification model of water-adulterated salmon. The clustering results were visualized and are illustrated in Figure 5(a). The hexagons represent competitive neurons, and the blue ones represent the winning neurons. The number of winning neurons is the number of adulterated salmon samples, and the number labeled in a neuron represents the number of samples in this type. Figure 5(a) shows that the combination of features of color moments and spectral values at feature wavelengths, functioning as the clustering attributes of the SOM network, divided the samples into four categories. The neurons 1–4 contained 18, 15, 17, and 10 samples, respectively. According to the identification results in Table 2, we could identify that two samples in the second category were misclassified into

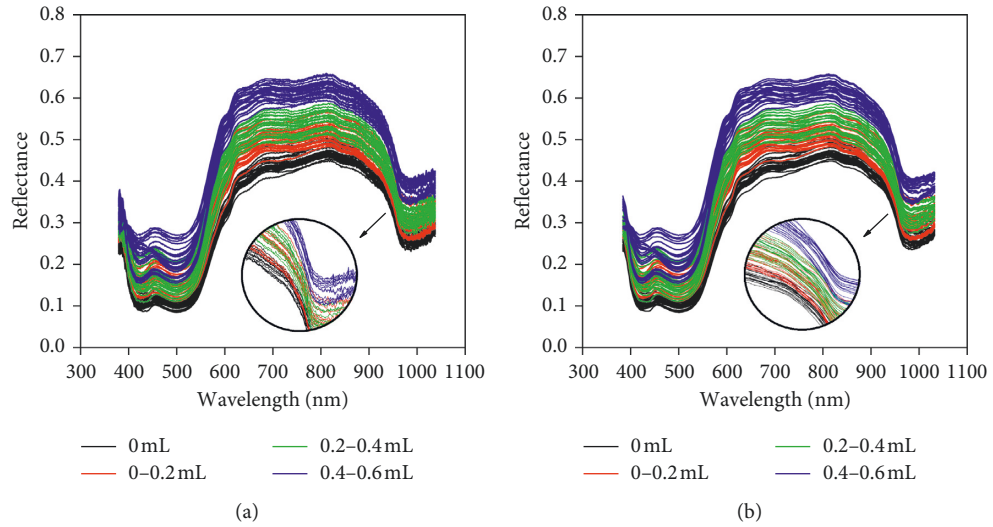

Figure 1: Averaged spectral profiles of salmon samples with (a) different water amounts injected and (b) different water amounts injected after SG smoothing.

Table 1: Principal-component eigenvalues and contribution rates of the salmon sample containing 0.3 mL of water.

PC	Eigenvalue	Contribution rate (%)	Cumulative contribution rate (%)
1	57.27692	87.41	87.41
2	7.906958	12.07	99.48
3	0.288961	0.44	99.92
4	0.022441	0.03	99.95
5	0.01744	0.03	99.98
6	0.015825	0.02	100

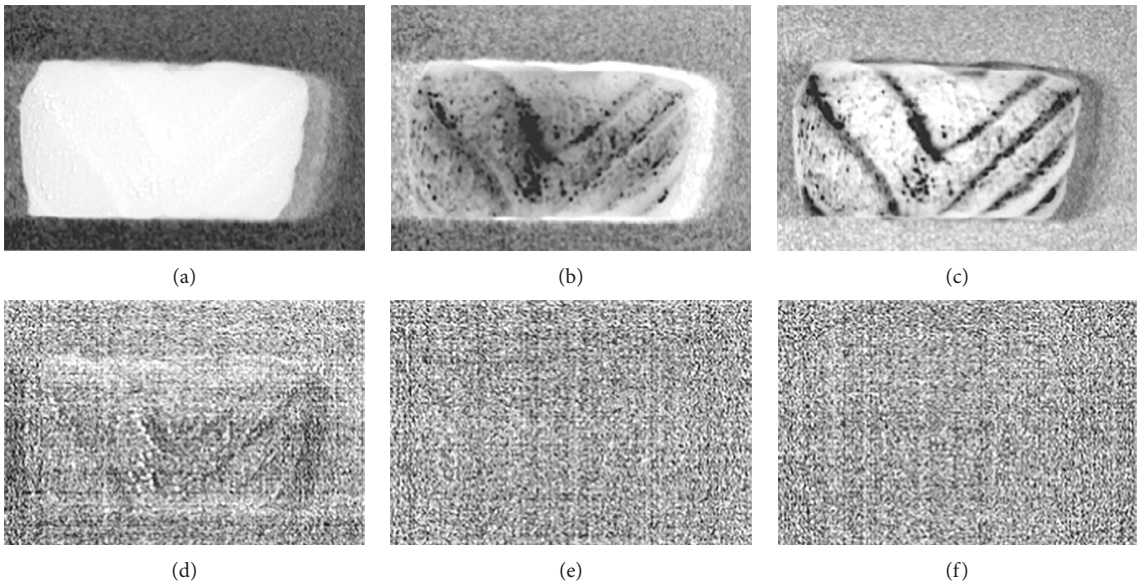

Figure 2: The first six principal-component images of the salmon sample with 0.3 mL of water injected: (a) PC1, (b) PC2, (c) PC3, (d) PC4, (e) PC5, and (f) PC6.

the first category; five samples in the second category were misclassified into the third category; and eight samples in the third category were misclassified into the second category. The total identification accuracy rate was 75%.

Figure 5(b) indicates the weight distances between neighboring neurons. The color blocks between the neuron nodes represent the distances between neuron weight vectors. The deeper the color is, the greater the distance is. The

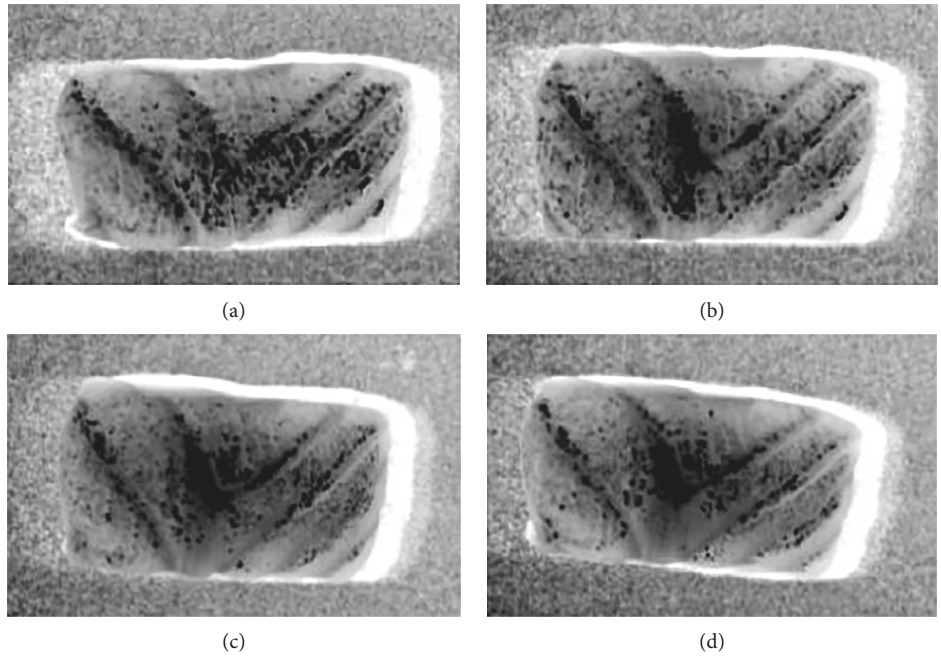

Figure 3: PC2 images of the salmon samples with (a) 0, (b) 0–0.2, (c) 0.2–0.4, and (d) 0.4–0.6 mL of water injected.

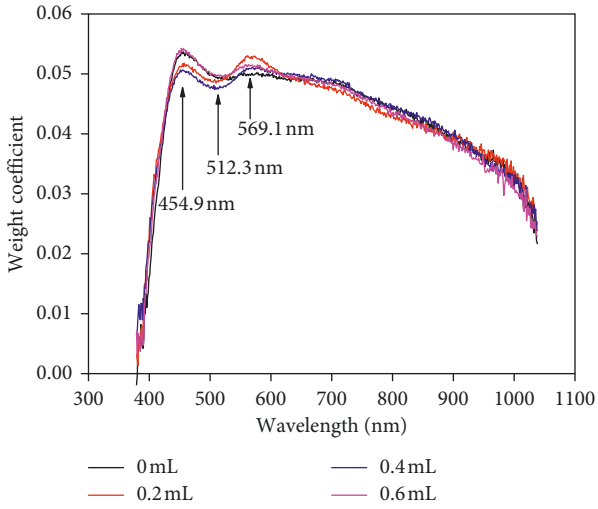

Figure 4: Weighting coefficients of the samples with different water amounts injected.

block between the cluster in neuron 3 (without water injected) and the cluster in neuron 2 (0.4–0.6 mL of water injected) is the deepest in color, which is consistent with the fact that meat color changed with the increase of water amount injected.

3.4.2. Water-Adulterated Salmon Identification Model Based on the Texture Features and Feature Spectra. The texture features (contrast, correlation, entropy, energy, and angular second-order moment) and spectral values at feature wavelengths (454.9, 512.3, and 569.1 nm) of sixty salmon samples were extracted and normalized. Normalized eight feature vectors were set as the input of the SOM network, and the SOM-based identification model of water-adulterated salmon was established.

The clustering results were visualized and are presented in Figure 6(a). The combination of texture features and spectral values at feature wavelengths, functioning as the clustering attributes of the SOM network, divided the samples into four categories. The neurons 1–4 contained 20, 16, 11, and 13 samples, respectively. As shown in Table 3, one sample in the second category was misclassified into the first category; one sample in the third category was misclassified into the second category; two samples in the second category and five samples in the fourth category were misclassified into the third category; and one sample in the third category was misclassified into the fourth category. The total identification accuracy rate was 83.3%.

Figure 6(b) indicates the weight distances between neighboring neurons. The neurons 2 and 4 are the closest, indicating that the texture and spectral features difference between the cluster in neuron 2 (first category, without water injected) and cluster in neuron 4 (second category, 0–0.2 mL of water injected) is the smallest. On the other hand, the neurons 2 and 3 have the farthest distance, demonstrating that the texture features difference between the cluster in neuron 2 and cluster in neuron 3 (fourth category, 0.4–0.6 mL of water injected) is the greatest, which is in accordance with the texture-change trend with the increase of water amount injected.

3.4.3. Water-Adulterated Salmon Identification Model Based on the Texture Features, Color Moment Features, and Feature Spectra. The texture features (contrast, correlation, entropy, energy, and angular second-order moment), color moment features (first- and second-order), and spectral values at

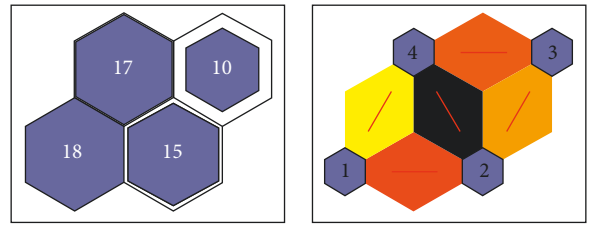

(a) (b)

Figure 5: (a) Visualized clustering results and (b) weight distances between adjacent neurons of the identification model of water-adulterated salmon based on feature spectra and features of color moments.

Table 2: The identification results.

Clustering center	Numbers of the samples	Category	Accuracy of identification
Neuron 1	16, 22, 23, 24, 27, 28, 29, 30, 31, 32, 35, 37, 38, 39, 42, 43, 44, and 45	Second	75%
Neuron 2	46, 47, 48, 49, 50, 51, 52, 53, 54, 55, 56, 57, 58, 59, and 60	Fourth	
Neuron 3	1, 2, 3, 4, 5, 6, 7, 8, 9, 10, 11, 12, 13, 14, 15, 17, and 22	First	
Neuron 4	18, 19, 21, 25, 26, 33, 34, 36, 40, and 41	Third	

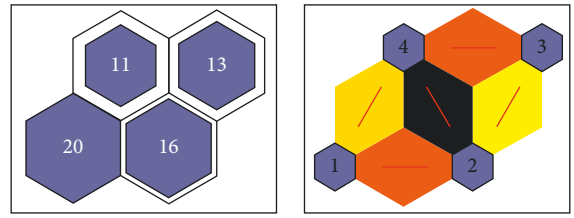

(a) (b)

Figure 6: (a) Visualized clustering results and (b) weight distances between adjacent neurons of the water-adulterated salmon identification model based on texture features and feature spectra.

Table 3: Identification results.

Clustering center	Numbers of the samples	Category	Accuracy of identification
Neuron 1	17, 26, 31, 32, 33, 36, 37, 38, 39, 40, 41, 42, 43, 44, 45, 47, 48, 54, 56, and 59	Third	83.3%
Neuron 2	1, 2, 3, 4, 5, 6, 7, 8, 9, 10, 11, 12, 13, 14, 15, and 20	First	
Neuron 3	34, 46, 49, 50, 51, 52, 53, 55, 57, 58, and 60	Fourth	
Neuron 4	16, 18, 19, 21, 22, 23, 24, 25, 27, 28, 29, 30, and 33	Second	

feature wavelengths (454.9, 512.3, and 569.1 nm) of sixty salmon samples were extracted and normalized. The normalized ten feature vectors were set as the input of the SOM network, and the SOM-based identification model of water-adulterated salmon was established.

Figure 7(a) demonstrates that the combination of color moment features, texture features, and spectral values at feature wavelengths, functioning as the clustering attributes of the SOM network, divided the samples into four categories. The neurons 1–4 contained 14, 16, 15, and 15 samples, respectively. As shown in Table 4, one sample in the second category was misclassified into the first category and one sample in the third category was misclassified into the second category. The total identification accuracy rate was 96.7%.

Through the self-organizing competition of the SOM network, the weight distances between neighboring neurons were quantified, as shown in Figure 7(b). The neurons 2 and 4 are the closest, indicating that the texture, color moment, and spectral features difference between the cluster in neuron 2 (first category, without water injected) and cluster in neuron 4 (second category, 0–0.2 mL of water injected)

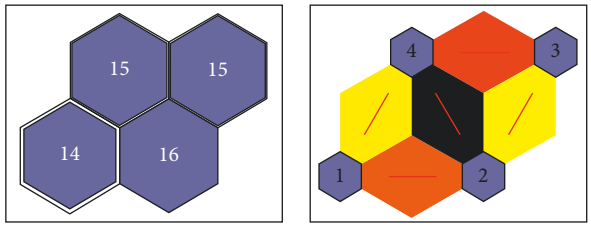

(a) (b)

Figure 7: (a) Visualized clustering results and (b) weight distances between adjacent neurons of the water-adulterated salmon identification model based on color moment features, texture features, and feature spectra.

Table 4: Identification results.

Clustering center	Numbers of the samples	Category	Accuracy of identification
Neuron 1	31, 32, 34, 35, 36, 37, 38, 39, 40, 41, 42, 43, 44, and 45	Third	96.7%
Neuron 2	1, 2, 3, 4, 5, 6, 7, 8, 9, 10, 11, 12, 13, 14, 15, and 20	First	
Neuron 3	46, 47, 48, 49, 50, 51, 52, 53, 54, 55, 56, 57, 58, 59, and 60	Fourth	
Neuron 4	16, 17, 18, 19, 21, 22, 23, 24, 25, 26, 27, 28, 29, 30, and 33	Second	

are the smallest. On the other hand, the neurons 2 and 3 have the farthest distance, demonstrating that the features difference between the cluster in neuron 2 and cluster in neuron 3 (fourth category, 0.4–0.6 mL of water injected) is the greatest, which is in accordance with the texture- and color-change trend with the increase of water amount injected.

According to the identification accuracy rate, the model based on the texture features, color moment features, and feature spectra has the best performance in identification (Table 4). Thereby, forty salmon samples were used as the prediction set for the model. As shown in Table 5, the accuracy rate of the prediction set was 95%. Compared with the modeling set, the accuracy of discrimination was slightly reduced. It indicated that the model based on the above three features has better robustness and identification accuracy.

4. Conclusions

A nondestructive detection method was developed based on hyperspectral technology for salmon adulteration. The hyperspectral images of salmon samples in the wavelength range of 390–1050 nm were acquired. Six principal-component images of the hyperspectral images in the wavelength range of 400–1000 nm were extracted via the PCA approach. The PC2 image was selected as the feature image, and the three feature wavelengths (454.9, 512.3, and 569.1 nm) were selected according to the weight coefficients of the feature image (PC2). The color moment features (first- and second-order), texture features (contrast, correlation, entropy, energy, and angular second-order moment), and spectral values at feature wavelengths were extracted for the establishment of SOM-based salmon adulteration identification models. The color moment features combined with spectral values at feature wavelengths, texture features combined with spectral values at feature wavelengths, and color-texture features combined with spectral values at feature wavelengths were separately selected as the input for the models. The results showed that the SOM-based model, with color-texture features combined with spectral values at feature wavelengths as the input, had the best performance in prediction. The identification accuracy rates of the modeling set and prediction set were 96.7% and 95%. On the theoretical and experimental basis of this work, rapid nondestructive identification of salmon adulteration technique and instruments will be further developed.

Table 5: Identification results.

Clustering center	Numbers of the samples	Category	Accuracy of identification
Neuron 1	P21, P22, P23, P24, P25, P26, P27, P28, P29, P30, and P31	Third	95%
Neuron 2	P1, P2, P3, P4, P5, P6, P7, P8, P9, P10, and P19	First	
Neuron 3	P32, P33, P34, P35, P36, P37, P38, P39, and P40	Fourth	
Neuron 4	P11, P12, P13, P14, P15, P16, P17, P18, and P20	Second	

Data Availability

The hyperspectral data used to support the findings of this study are available from the corresponding author upon request.

Conflicts of Interest

The authors declare that they have no conflicts of interest.

Acknowledgments

This work was supported by the National Key Research and Development Project of China (2018YFD0700905), National Natural Science Foundation of China (31701696), Innovative Support Program for High-level Personnel of Da Lian (2017RQ128), and the Science and Technology Project of Liaoning Province (201602055, 20180551017, and 20180550454).

References

[1] T. A. Mori, R. Vandongen, L. J Beilin, V. Burke, J. Morris, and J. Ritchie, "Effects of varying dietary fat, fish, and fish oils on blood lipids in a randomized controlled trial in men at risk of heart disease," *American Journal of Clinical Nutrition*, vol. 59, no. 5, pp. 1060–1068, 1994.

[2] X. Zang, Z. Lin, T. Zhang et al., "Non-destructive measurement of water and fat contents, water dynamics during drying

and adulteration detection of intact small yellow croaker by low field NMR," *Journal of Food Measurement and Characterization*, vol. 11, no. 4, pp. 1550–1558, 2017.

[3] F. J. P. Elortondo, M. Ojeda, M. Albisu, J. Salmerón, I. Etayo, and M. Molina, "Food quality certification: an approach for the development of accredited sensory evaluation methods," *Food Quality and Preference*, vol. 18, no. 2, pp. 425–439, 2007.

[4] U. Samarajeewa, A. C. Sen, M. D. Cohen, and C. I. Wei, "Detoxification of aflatoxins in foods and feeds by physical and chemical methods," *Journal of Food Protection*, vol. 53, no. 6, pp. 489–501, 1990.

[5] K. L. Pearce, K. Rosenvold, H. J. Andersen, and D. L. Hopkins, "Water distribution and mobility in meat during the conversion of muscle to meat and ageing and the impacts on fresh meat quality attributes-a review," *Meat Science*, vol. 89, no. 2, pp. 111–124, 2011.

[6] W. Timothy, N. Gavin, B. Claire, A. Waltho, A. Alroichdi, and M. Burns, "Feasibility study for applying spectral imaging for wheat grain authenticity testing in pasta," *Food and Nutrition Sciences*, vol. 7, no. 5, pp. 355–361, 2016.

[7] F. Han, X. Huang, E. Teye, H. Gu, H. Dai, and L. Yao, "A nondestructive method for fish freshness determination with electronic tongue combined with linear and non-linear multivariate algorithms," *Czech Journal of Food Sciences*, vol. 32, no. 6, pp. 532–537, 2014.

[8] J. H. Cheng, D. W. Sun, X. A. Zeng, and H. B. Pu, "Nondestructive and rapid determination of TVB-N content for freshness evaluation of grass carp (Ctenopharyngodon idella) by hyperspectral imaging," *Innovative Food Science and Emerging Technologies*, vol. 21, no. 4, pp. 179–187, 2014.

[9] M. Kamruzzaman, S. Y. Makino, and S. Oshita, "Rapid and non-destructive detection of chicken adulteration in minced beef using visible near-infrared hyperspectral imaging and machine learning," *Journal of Food Engineering*, vol. 170, no. 7, pp. 8–15, 2016.

[10] J. H. Cheng and D. W. Sun, "Rapid quantification analysis and visualization of Escherichia coli loads in grass carp fish flesh by hyperspectral imaging method," *Food and Bioprocess Technology*, vol. 8, no. 5, pp. 951–959, 2015.

[11] H. Pu, D. W. Sun, J. Ma, and J. H. Cheng, "Classification of fresh and frozen-thawed pork muscles using visible and near infrared hyperspectral imaging and textural analysis," *Meat Science*, vol. 99, pp. 81–88, 2015.

[12] F. A. Mianji, Y. Zhang, and A. Babakhani, "Key information retrieval in hyperspectral imagery through spatial-spectral data fusion," *Radioengineering*, vol. 19, no. 4, pp. 186–193, 2010.

[13] T. Li, H. Mei, and P. Cong, "Combining nonlinear PLS with the numeric genetic algorithm for QSAR," *Chemometrics and Intelligent Laboratory Systems*, vol. 45, no. 1-2, pp. 177–184, 1999.

[14] J. H. Cheng, D. W. Sun, and H. Pu, "Combining the genetic algorithm and successive projection algorithm for the selection of feature wavelengths to evaluate exudative characteristics in frozen-thawed fish muscle," *Food Chemistry*, vol. 197, pp. 855–863, 2016.

[15] H. Min, X. Wan, Z. Min, and Q. Zhu, "Detection of insect-damaged vegetable soybeans using hyperspectral transmittance image," *Journal of Food Engineering*, vol. 116, no. 1, pp. 45–49, 2013.

[16] J. Wang, K. Nakano, S. Ohashi, Y. Kubota, K. Takizawa, and Y. Sasaki, "Detection of external insect infestations in jujube fruit using hyperspectral reflectance imaging," *Biosystems Engineering*, vol. 108, no. 4, pp. 345–351, 2011.

[17] J.-H. Cheng, D.-W. Sun, H.-B. Pu, Q.-J. Wang, and Y.-N. Chen, "Suitability of hyperspectral imaging for rapid evaluation of thiobarbituric acid (TBA) value in grass carp (Ctenopharyngodon idella) fillet," *Food Chemistry*, vol. 171, no. 4, pp. 258–265, 2015.

[18] M. Huang, M. S. Kim, S. R. Delwiche et al., "Quantitative analysis of melamine in milk powders using near-infrared hyperspectral imaging and band ratio," *Journal of Food Engineering*, vol. 181, pp. 10–19, 2016.

[19] G. Bázár, R. Romvári, A. Szabó, T. Somogyi, V. Éles, and R. Tsenkova, "NIR detection of honey adulteration reveals differences in water spectral pattern," *Food Chemistry*, vol. 194, pp. 873–880, 2016.

[20] J. B. Li, X. Q. Rao, and Y. B. Ying, "Advance on application of hyperspectral imaging to nondestructive detection of agricultural products external quality," *Spectroscopy and Spectral Analysis*, vol. 31, no. 8, p. 2021, 2011.

[21] M. Kamruzzaman, D. W. Sun, G. ElMasry, and P. Allen, "Fast detection and visualization of minced lamb meat adulteration using NIR hyperspectral imaging and multivariate image analysis," *Talanta*, vol. 103, no. 2, pp. 130–136, 2013.

[22] M. Kamruzzaman, Y. Makino, S. Oshita, and S. Liu, "Assessment of visible near-infrared hyperspectral imaging as a tool for detection of horsemeat adulteration in minced beef," *Food and Bioprocess Technology*, vol. 8, no. 5, pp. 1054–1062, 2015.

[23] W. Di, S. Hui, H. Yong, X. Yu, and Y. Bao, "Potential of hyperspectral imaging and multivariate analysis for rapid and non-invasive detection of gelatin adulteration in prawn," *Journal of Food Engineering*, vol. 119, no. 3, pp. 680–686, 2013.

[24] G. Javier, S. A. Hale, and S. M. Blanchard, "Quantitative analysis and detection of adulteration in crab meat using visible and near-infrared spectroscopy," *Journal of Agricultural and Food Chemistry*, vol. 54, no. 4, pp. 1130–1136, 2006.

[25] D. Manolakis and G. Shaw, "Detection algorithms for hyperspectral imaging applications," *IEEE Signal Processing Magazine*, vol. 19, no. 1, pp. 29–43, 2002.

[26] B. Mojaradi, H. Abrishami-Moghaddam, M. J. V. Zoej, and R. P. W. Duin, "Dimensionality reduction of hyperspectral data via spectral feature extraction," *IEEE Transactions on Geoscience and Remote Sensing*, vol. 47, no. 7, pp. 2091–2105, 2009.

[27] C. I. Chang and H. Ren, "An experiment-based quantitative and comparative analysis of target detection and image classification algorithms for hyperspectral imagery," *IEEE Transactions on Geoscience and Remote Sensing*, vol. 38, no. 2, pp. 1044–1063, 2000.

[28] Y. Zhao, C. Zhang, S. Zhu, P. Gao, L. Feng, and Y. He, "Non-destructive and rapid variety discrimination and visualization of single grape seed using near-infrared hyperspectral imaging technique and multivariate analysis," *Molecules*, vol. 23, no. 6, p. 1352, 2018.

[29] J. H. Cheng, D. W. Sun, H. B. Pu et al., "Integration of classifiers analysis and hyperspectral imaging for rapid discrimination of fresh from cold-stored and frozen-thawed fish fillets," *Journal of Food Engineering*, vol. 161, no. 6, pp. 33–39, 2015.

[30] H. Sun, T. Zheng, N. Liu, M. Cheng, M. Li, and Q. Zhang, "Vertical distribution of chlorophyll in potato plants based on hyperspectral imaging," *Transactions of the Chinese Society of Agricultural Engineering*, vol. 34, no. 1, pp. 149–156, 2018.

[31] J. Xie, T. Pan, J. M. Chen, H. Z. Chen, and X. H. Ren, "Joint optimization of savitzky-golay smoothing models and partial least squares factors for near-infrared spectroscopic analysis

of serum glucose," *Chinese Journal of Analytical Chemistry (Chinese Version)*, vol. 38, no. 3, pp. 342–346, 2010.

[32] B. M. Wise, N. L. Ricker, D. F. Veltkamp, and B. R. Kowalski, "A. Theoretical basis for the use of principal component models for monitoring multivariate processes," *Process Control and Quality*, vol. 1, no. 1, 1990.

[33] T. Lei, Y. Fan, and Y. Wang, "Colour edge detection based on the fusion of hue component and principal component analysis," *IET Image Processing*, vol. 8, no. 1, pp. 44–55, 2014.

[34] X. Jia and J. A. Richards, "Segmented principal components transformation for efficient hyperspectral remote-sensing image display and classification," *IEEE Transactions on Geoscience and Remote Sensing*, vol. 37, no. 1, pp. 538–542, 1999.

[35] W. Hou, J. Wang, X. Xu, J. S. Reid, and D. Han, "An algorithm for hyperspectral remote sensing of aerosols: 1. Development of theoretical framework," *Journal of Quantitative Spectroscopy and Radiative Transfer*, vol. 178, pp. 400–415, 2016.

[36] I. Champion, C. Germain, J. P. D. Costa, A. Alborini, and P. Dubois-Fernandez, "Retrieval of forest stand age from SAR image texture for varying distance and orientation values of the gray level Co-occurrence matrix," *IEEE Geoscience and Remote Sensing Letters*, vol. 11, no. 1, pp. 5–9, 2013.

[37] S. N. Ondimu and H. Murase, "Effect of probability-distance based Markovian texture extraction on discrimination in biological imaging," *Computers and Electronics in Agriculture*, vol. 63, no. 1, pp. 2–12, 2008.

[38] B. Park, K. C. Lawrence, W. R. Windham, Y. R. Chen, and K. Chao, "Discriminant analysis of dual-wavelength spectral images for classifying poultry carcasses," *Computers and Electronics in Agriculture*, vol. 33, no. 3, pp. 219–231, 2002.

[39] O. Sertel, J. Kong, H. Shimada, U. V. Catalyurek, J. H. Saltz, and M. N. Gurcan, "Computer-aided prognosis of neuroblastoma on whole-slide images: classification of stromal development," *Pattern Recognition*, vol. 42, no. 6, pp. 1093–1103, 2009.

[40] R. M. Haralick, "Statistical and structural approaches to texture," *Proceedings of the IEEE*, vol. 67, no. 5, pp. 786–804, 2005.

[41] Q. Zhu, M. Huang, R. Lu, and F. Mendoza, "Analysis of hyperspectral scattering images using a moment method for apple firmness prediction," *Transactions of the ASABE*, vol. 57, no. 1, pp. 75–83, 2014.

[42] E. Nuno, R. Ortega, L. Basanez, and D. Hill, "Synchronization of networks of nonidentical euler-Lagrange systems with uncertain parameters and communication delays," *IEEE Transactions on Automatic Control*, vol. 56, no. 4, pp. 935–941, 2011.

[43] H. Sang, A. E. Gelfand, C. Lennard, G. Hegerl, and B. Hewitson, "Interpreting self-organizing maps through space-time data models," *Annals of Applied Statistics*, vol. 2, no. 4, pp. 1194–1216, 2008.

[44] S. Atilgan, Z. Ekmekci, A. L. Dogan, D. Guc, and E. U. Akkaya, "Water soluble distyryl-boradiazaindacenes as efficient photosensitizers for photodynamic therapy," *Chemical Communications*, vol. 42, pp. 4398–4400, 2006.

[45] S. Bayen, X. Yi, E. Segovia, Z. Zhou, and B. C. Kelly, "Analysis of selected antibiotics in surface freshwater and seawater using direct injection in liquid chromatography electrospray ionization tandem mass spectrometry," *Journal of Chromatography A*, vol. 1338, no. 5, pp. 38–43, 2014.

[46] K. J. Zuzak, S. C. Naik, G. Alexandrakis, D. Hawkins, K. Behbehani, and E. Livingston, "Intraoperative bile duct visualization using near-infrared hyperspectral video imaging," *American Journal of Surgery*, vol. 195, no. 4, pp. 491–497, 2008.

[47] Y. Zhou, S. G. Dai, J. Lu, T. B. Liu, and Y. Shi, "Effect of spectral pretreatment on near infrared spectroscopy for rapid detection of wine alcohol," *Opto-Electronic Engineering*, vol. 38, no. 4, pp. 54–58, 2011.

[48] H. Lian, "On feature selection with principal component analysis for one-class SVM," *Pattern Recognition Letters*, vol. 33, no. 9, pp. 1027–1031, 2012.

[49] R. Maia, C. M. Eliason, P. P. Bitton, S. M. Doucet, and M. D. Shawkey, "Pavo:an R package for analysis, visualization and organization of spectral color data," *Methods in Ecology and Evolution*, vol. 4, no. 10, pp. 906–913, 2013.

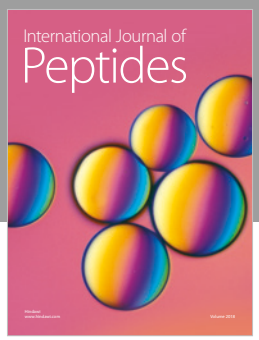

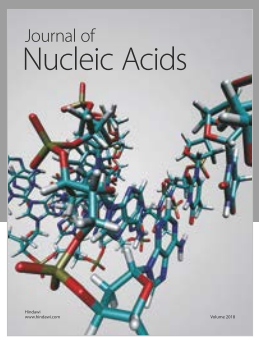

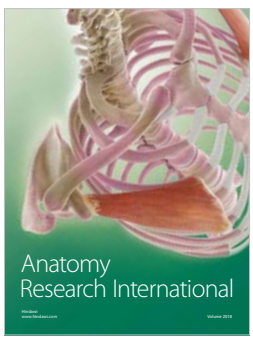

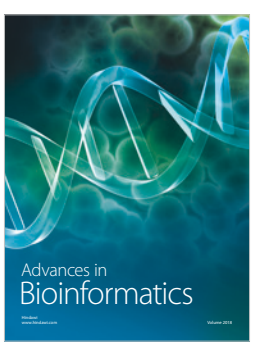

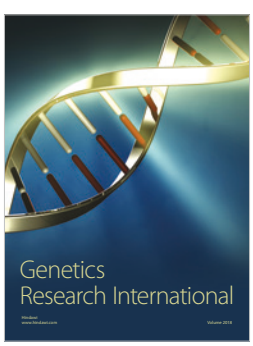

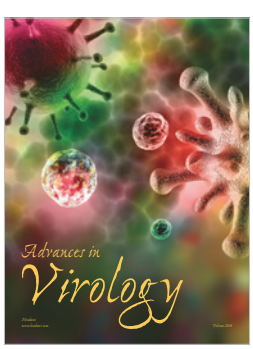

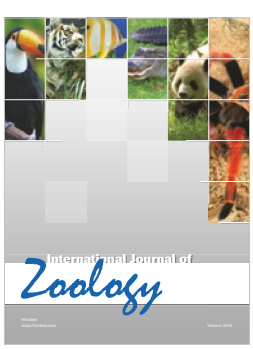

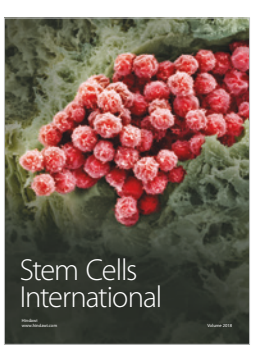

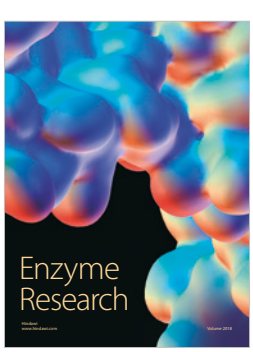

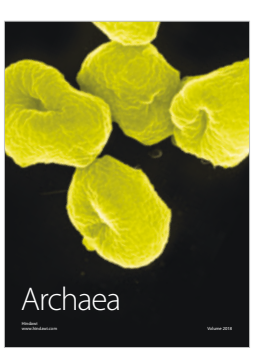


Hindawi

Submit your manuscripts at
www.hindawi.com